Inorganic Chemistry

Article

pubs.acs.org/IC

Synthesis and Structural Characterization of a Series of $Mn^{III}OR$ Complexes, Including a Water-Soluble $Mn^{III}OH$ That Promotes Aerobic Hydrogen-Atom Transfer

Michael K. Coggins, Lisa M. Brines, and Julie A. Kovacs*

Department of Chemistry, University of Washington, Box 351700, Seattle, Washington 98195-1700, United States

Supporting Information

ABSTRACT: Hydrogen-atom-transfer (HAT) reactions are a class of proton-coupled electron-transfer (PCET) reactions used in biology to promote substrate oxidation. The driving force for such reactions depends on both the oxidation potential of the catalyst and the pK_a value of the proton-acceptor site. Both high-valent transition-metal oxo M^{IV}=O (M = Fe, Mn) and lower-valent transition-metal hydroxo compounds M^{III}OH (M = Fe, Mn) have been shown to promote these reactions. Herein we describe the synthesis, structure, and reactivity properties of a series of Mn^{III}OR compounds [R = $^{p}NO_2$Ph (**5**), Ph (**6**), Me (**7**), H (**8**)], some of which abstract H atoms. The Mn^{III}OH complex **8** is water-soluble and represents a rare example of a stable mononuclear Mn^{III}OH. In water, the redox potential of **8** was found to be pH-dependent and the Pourbaix ($E_{p,c}$ vs pH) diagram has a slope (52 mV pH^{-1}) that is indicative of the transfer a single proton with each electron (i.e., PCET). The two compounds with the lowest oxidation potential, hydroxide- and methoxide-bound **7** and **8**, are found to oxidize 2,2′,6,6′-tetramethylpiperidin-1-ol (TEMPOH), whereas the compounds with the highest oxidation potential, phenol-ligated **5** and **6**, are shown to be unreactive. Hydroxide-bound **8** reacts with TEMPOH an order of magnitude faster than methoxide-bound **7**. Kinetic data [k_H/k_D = 3.1 (**8**); k_H/k_D = 2.1 (**7**)] are consistent with concerted H-atom abstraction. The reactive species **8** can be aerobically regenerated in H_2O, and at least 10 turnovers can be achieved without significant degradation of the "catalyst". The linear correlation between the redox potential and pH, obtained from the Pourbaix diagram, was used to calculate the bond dissociation free energy (BDFE) = 74.0 ± 0.5 kcal mol^{-1} for $Mn^{II}OH_2$ in water, and in MeCN, its BDFE was estimated to be 70.1 kcal mol^{-1}. The reduced protonated derivative of **8**, $[Mn^{II}(S^{Me2}N_4(tren))(H_2O)]^+$ (**9**), was estimated to have a pK_a of 21.2 in MeCN. The ability (**7**) and inability (**5** and **6**) of the other members of the series to abstract a H atom from TEMPOH was used to estimate either an upper or lower limit to the Mn^{II}O(H)R pK_a based on their experimentally determined redox potentials. The trend in pK_a [21.2 (R = H) > 16.2 (R = Me) > 13.5 (R = Ph) > 12.2 (R = $^{p}NO_2$Ph)] is shown to oppose that of the oxidation potential $E_{p,c}$ [−220 (R = $^{p}NO_2$Ph) > −300 (R = Ph) > −410 (R = Me) > −600 (R = H) mV vs $Fc^{+/0}$] for this particular series.

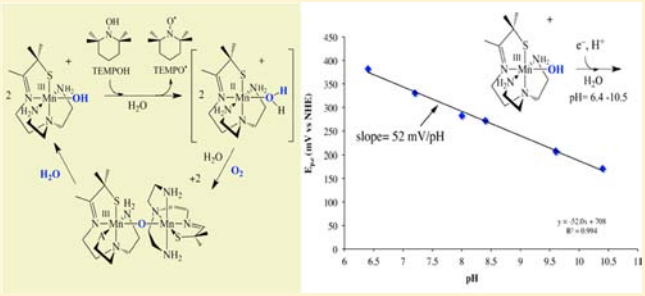

INTRODUCTION

Hydrogen-atom (H•)-transfer (HAT) reactions are a class of proton-coupled electron-transfer (PCET) reactions used in biology to promote substrate oxidation.[1,2] Typically, these reactions are catalyzed by reactive intermediates formed upon the addition of dioxygen (O_2) to reduced transition-metal ions (e.g., Fe, Cu, Mn). When strong C−H bonds are involved, one would anticipate that the reactive catalyst would have to be highly oxidizing and therefore high-valent, e.g., M^{IV}=O (M = Mn, Fe).[3−6] In some cases, however, a lower-valent M^{III}OH (M = Mn, Fe) has been shown to activate C−H bonds, an example of which is lipoxygenase (Figure 1). Lipoxygenases convert α-linoleic acid to hydroperoxyoctadecatreienoic acid via the homolytic cleavage of an, albeit weaker (bond dissociation energy, BDE ∼ 77 kcal mol^{-1}),[7] allylic C−H bond. The thermodynamic driving force for oxidation reactions of this type depends on the relative strength of the substrate X−H (X = C, N, O) versus catalyst M^{II}(HO−H) or M^{III}(O−H) bond.[1,8−12] One can relate this driving force to both the redox potential [$E_{1/2}(M^{III}/M^{II})$ or $E_{1/2}(M^{IV}/M^{III})$] and basicity of the M^{III}OH or M^{IV}=O oxygen.[1] As long as the coordinated O atom is basic enough, then the oxidant can be rather mild (i.e., possess a low $E_{1/2}$) and still capable of promoting H-atom abstraction. The increased basicity of a lower-valent M^{III}OH oxygen versus higher-valent M(IV)=O oxygen could conceivably offset the expected decrease in the redox potential caused by the decrease in the oxidation state, and this might explain the ability of M^{III}OH species to abstract H atoms. A recent study addresses this point by comparing the thermodynamics and kinetics of H-atom abstraction by structurally analogous synthetic $LMn^{IV}(O)_2$, $LMn^{IV}(O)(OH)^+$,

Received: May 16, 2013
Published: October 24, 2013

   dx.doi.org/10.1021/ic401234t | Inorg. Chem. 2013, 52, 12383−12393

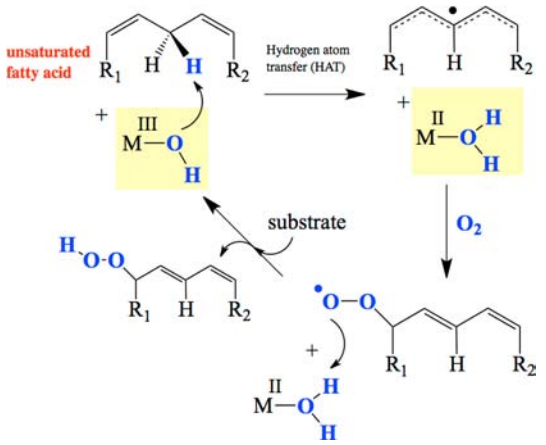

Figure 1. Reaction scheme showing the mechanism of lipoxygenase substrate oxidation, which involves abstraction of an allylic H atom from the substrate by a catalytically active $M^{III}OH$ (M = Mn, Fe).

$LMn^{IV}(OH)(OH)^{2+}$, and $LMn^{IV}(OH)(OH_2)^{3+}$ complexes.[13−16] This study shows that the H-atom-abstracting capability of Mn^{IV}═O and Mn^{IV}OH is approximately the same because the oxidation potential decrease is offset by an increase in pK_a. This compensation effect is also observed upon sequential deprotonation of coordinated water molecules. The kinetics of hydrogen atom transfer is influenced by the protonation state in this particular series of molecules, however: Mn(IV)═O reacts ∼40 times faster than Mn(IV)—OH. Thiolate ligands have also been shown to facilitate biological HAT by creating a more basic oxo.[17−20] We are interested in developing these ideas further by exploring the HAT reactivity of thiolate-ligated small-molecule systems. Herein, we describe the synthesis and properties of a series of thiolate- ligated $Mn^{III}OR$ compounds. By altering the R group, we are able to influence the pK_a value of the coordinated ROH and determine how this influences the HAT capability. Included in this study is the reactivity of a rare example of a *water-soluble* thiolate-ligated *$Mn^{III}OH$ that abstracts $H^{\bullet}$ from organic substrates*. A thermochemical cycle is used to obtain quantitative data and determine the relative influence of the redox potential versus pK_a in driving the observed HAT reaction in both water and acetonitrile.

EXPERIMENTAL SECTION

General Methods. All manipulations were performed using Schlenk-line techniques or under a dinitrogen atmosphere in a glovebox. Reagents and solvents purchased from commercial vendors were of the highest available purity and were used without further purification unless otherwise noted. MeOH (Na) and MeCN (CaH_2) were dried and distilled prior to use. Et_2O was rigorously degassed and purified using solvent purification columns housed in a custom stainless steel cabinet and dispensed by a stainless steel Schlenk-line (GlassContour). IR spectra were recorded as Nujol mulls on NaCl salt plates with a Perkin-Elmer 1720 FT-IR spectrometer. UV/vis spectra were recorded on a Varian Cary 50 spectrophotometer equipped with a fiber-optic cable connected to a "dip" ATR probe (C-technologies). A custom-built two-neck solution sample holder equipped with a threaded glass connector was sized specifically to fit the "dip" probe. Electron paramagnetic resonance (EPR) spectra were recorded between 5 and 7 K on a Varian continuous-wave EPR spectrometer equipped with an Oxford helium cryostat. Magnetic moments (solid state) were obtained with polycrystalline samples in gel caps from 5 to 300 K by zero-field-cooled experiments using a Quantum Design MPMS S5 SQUID magnetometer. Pascal's constants were used to correct for diamagnetic contributions to the experimental magnetic moment. Solution magnetic moments were determined using the Evans method,[21] with temperature correction made in the manner described by Van Geet.[22] Cyclic voltammograms were recorded in either MeCN [100 mM $^{n}Bu_4N(PF_6)$ supporting electrolyte] or H_2O (100 mM $KClO_4$ supporting electrolyte) on a PAR 263A potentiostat utilizing a glassy carbon working electrode, a platinum auxiliary electrode, and a Ag^+/Ag reference electrode. pH measurements were made using a Beckman Coulter 400 series hand-held meter. X-ray crystallography data were recorded on a Bruker APEX II single-crystal X-ray diffractometer with Mo radiation. Elemental analyses were performed by Atlantic Microlabs (Norcross, GA). 2,2′,6,6′-Tetramethylpiperidin-1-ol (TEMPOH)[23] and $[Mn^{II}(S^{Me2}N_4(tren))](PF_6)$ (**1**)[24] were prepared according to literature procedures.

Synthesis of $[Mn^{III}(S^{Me2}N_4(tren))_2$-$(\mu$-O)$](PF_6)_2$·MeCN (2). An anaerobic MeCN solution (5 mL) of **1**[24] (500 mg, 1.12 mmol), containing the $S^{Me2}N_4$(tren) ligand, was prepared in a drybox. The solution was removed from the drybox and exposed to air for 5 min. The removal of all volatiles in vacuo afforded the title compound as a purple solid in nearly quantitative yield (499 mg, 0.55 mmol). Electronic absorption [MeCN; λ_{max}, nm (ε, M^{-1} cm^{-1})]: 535 (510), 600 (380). Magnetic moment (299 K, solution state, CD_3CN): 2.86 μ_B per Mn. Elem anal. Calcd for $C_{22}H_{50}N_8OF_{12}P_2S_2Mn_2$: C, 29.15; H, 5.56; N, 12.36. Found: C, 28.19; H, 5.40; N, 12.28.

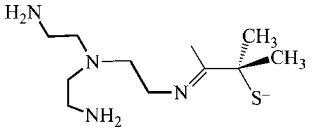

$S^{Me2}N_4$(tren)

Synthesis of $[Mn^{III}(S^{Me2}N_4(tren)(OPh$-$^{p}NO_2))](PF_6)$·MeCN (5). An anaerobic MeCN solution (2 mL) of **2** (100 mg, 0.110 mmol) was prepared in a drybox. An excess of $^{p}NO_2PhOH$ (765 mg, 5.50 mmol) was added as a solid to this solution. After the resulting solution was allowed to stir at room temperature for 10 min, all volatiles were removed in vacuo to afford a black solid. The resulting solid was recrystallized twice from MeCN/Et_2O (1:5, v/v) to afford the title compound as a dark-red solid in 95% yield (122 mg, 0.210 mmol). Electronic absorption [MeCN; λ_{max}, nm (ε, M^{-1} cm^{-1})]: 395 (1180), 460 (820). Magnetic moment (299 K, solution state, CD_3CN): 4.80 μ_B. Elem anal. Calcd for $C_{17}H_{29}N_5O_3F_6PSMn$: C, 35.00; H, 5.01. Found: C, 35.49; H, 5.21.

Synthesis of $[Mn^{III}(S^{Me2}N_4(tren)(OPh))](PF_6)$·$Et_2O$·MeCN (6). An anaerobic MeCN solution (2 mL) of **2** (100 mg, 0.110 mmol) was prepared in a drybox. An excess of PhOH (1.04 g, 11.0 mmol) was added as a solid to this solution. After the resulting solution was allowed to stir at room temperature for 10 min, all volatiles were removed in vacuo to afford a dark-red solid. The resulting solid was recrystallized twice from MeCN/Et_2O (1:5, v/v) to afford the title compound as a red solid in 89% yield (106 mg, 0.200 mmol). Electronic absorption [MeCN; λ_{max}, nm (ε, M^{-1} cm^{-1})]: 506 (370), 820 (50). Magnetic moment (299 K, solution state, CD_3CN): 4.88 μ_B. Elem anal. Calcd for $C_{17}H_{30}N_4OF_6PSMn$: C, 37.92; H, 5.62; N, 10.41. Found: C, 38.00; H, 5.70; N, 10.49.

Synthesis of $[Mn^{III}(S^{Me2}N_4(tren)(OMe))](PF_6)$ (7). An anaerobic MeOH solution (1 mL) of **1** (100 mg, 0.224 mmol) was prepared in a drybox. The solution was removed from the drybox and exposed to air for 5 min. The removal of all volatiles in vacuo afforded the title compound as a red solid in nearly quantitative yield (106 mg, 0.222 mmol). Electronic absorption [MeCN; λ_{max}, nm (ε, M^{-1} cm^{-1})]: 342 (410), 439 (330), 510 (250), 768 (85). Magnetic moment (299 K, solution state, CD_3CN): 4.99 μ_B. Elem anal. Calcd for $C_{12}H_{28}N_4OF_6PSMn$: C, 30.26; H, 5.92; N, 11.76. Found: C, 30.29; H, 5.56; N, 11.61.

Synthesis of $[Mn^{III}(S^{Me2}N_4(tren))(OH)](PF_6)$·$H_2O$ (8). A 1 mL anaerobic aqueous solution of **1** (500 mg, 1.12 mmol) was prepared in a drybox. The solution was then removed from the drybox, opened to air, and allowed to stir at room temperature for 2−3 min. The removal of the volatiles in vacuo afforded the title compound as a red solid in

dx.doi.org/10.1021/ic401234t | *Inorg. Chem.* 2013, 52, 12383−12393

Table 1. Crystal Data for 2 and 5−8

	2	5	6	7	8
formula	$C_{24}H_{53}F_{12}Mn_2N_9OP_2S_2$	$C_{19}H_{32}F_6Mn\ N_6O_3PS$	$C_{23}H_{43}F_6Mn\ N_5O_2PS$	$C_{12}H_{28}F_6MnN_4OPS$	$C_{11}H_{28}F_6MnN_4O_2PS$
MW	947.69	624.48	653.59	476.35	480.35
T, K	130(2)	100(2)	110(2)	100(2)	100(2)
unit cell[a]	orthorhombic	monoclinic	monoclinic	orthorhombic	monoclinic
a, Å	12.5660(2)	31.099(2)	8.4834(3)	13.5710(19)	8.5318(6)
b, Å	17.0110(4)	14.0709(8)	16.4970(7)	8.8115(12)	16.6962(13)
c, Å	36.2170(6)	12.1715(7)	22.0354(9)	16.452(2)	13.7039(10)
α, deg	90	90	90	90	90
β, deg	90	91.213(4)	97.872(2)	90	94.552(3)
γ, deg	90	90	90	90	90
V, Å^3	7741.8(3)	5324.9(6)	3054.8(2)	1967.4(5)	1945.9(2)
Z	8	8	4	4	4
d(calcd), g cm^{-3}	1.626	1.558	1.421	1.608	1.640
space group	*Pbca*	*C*2/*c*	$P2_1/c$	*Pnma*	$P2_1/c$
R^b	0.0875	0.0506	0.0265	0.0494	0.0211
$R_w{}^b$	0.2476	0.1099	0.0668	0.1339	0.0559
GOF	1.014	1.169	1.041	1.077	1.042

[a]In all cases, Mo Kα (λ = 0.71070 Å) radiation. [b]$R = \sum||F_o| - |F_c||/\sum|F_o|$; $R_w = [\sum w(|F_o| = |F_c|)^2/\sum wF_o{}^2]^{1/2}$, where $w^{-1} = [\sigma_{count}{}^2 + (0.05F^2)^2]/4F^2$.

quantitative yield (518 mg, 1.12 mmol). Single crystals of **8** were grown from a 1:6 mixture of MeCN/Et_2O at 0 °C overnight. Solid **8** was stored at −80 °C to avoid small amounts of decomposition that occurs over a 24 h period at room temperature. Electronic absorption [H_2O; λ_{max}, nm (ε, M^{-1} cm^{-1})]: 287 (3720), 418 (229), 489 (364), 680 (25). Electronic absorption [MeCN; λ_{max}, nm (ε, M^{-1} cm^{-1})]: 299 (2221), 411 (260), 500 (320), 803 (40). IR (Nujol): ν_{O-H} 3367, ν_{O-D} 2457, $\nu_{C=N}$ 1585 cm^{-1}. Magnetic moment (299 K, solution state, CD_3CN): 4.89 μ_B. Elem anal. Calcd for $C_{11}H_{26}N_4OF_6PSMn$: C, 28.58; H, 5.67; N, 12.12. Found: C, 28.43; H, 5.43; N, 11.37.

Reaction between 8 or 7 and TEMPOH. In a typical reaction, a 1 mM solution of **7** or **8** was prepared in 4 mL of either H_2O or MeCN under an inert atmosphere in a drybox. The solution was transferred via a gastight syringe to a custom-made two-neck vial equipped with a septum cap and threaded dip-probe feed-through adaptor that had previously been purged with argon and contained a stir bar. The anaerobic solution of **7** or **8** was continuously stirred, while 0.2 equiv aliquots of a TEMPOH solution (0.1 M stock solution prepared in the appropriate solvent) were added to the reaction mixture. Stirring was discontinued 5 min following the addition of an aliquot of TEMPOH in order to record a UV/vis absorption spectrum. It was observed that all of the absorption bands characteristic of **7** or **8** decreased in a uniform fashion upon the addition of TEMPOH to the reaction mixture, with 1.0 equiv of TEMPOH resulting in the complete disappearance of all visible region absorption features. The resulting spectrum following the addition of 1.0 equiv of TEMPOH was compared to, and matched with, the reported absorption spectrum of the reduced manganese complex $[Mn^{II}(S^{Me2}N_4(tren))]^+$.[24]

Kinetic Measurements of 8- and 7-Promoted H-Atom Abstraction from TEMPOH(D). In a typical experiment, 3 mL of a 0.5 mM solution of **7** or **8** was prepared in a drybox and injected via a gastight syringe into a custom-made two-neck vial. The vial was equipped with a septum cap and threaded dip-probe feed-through adaptor that had previously been purged with argon and contained a stir bar. A known excess amount of TEMPOH(D) (0.1 mM stock solution in MeCN) was then injected into the solution containing **7** or **8**. Reaction progress was independently monitored by changes in the absorption intensity at 511 (**8**) and 520 nm (**7**), respectively, until no further change in the absorption intensity persisted for at least 60 s. First-order rate constants were calculated by plotting $\ln[(A_t - A_f)/A_0 - A_f)]$ versus time. Experiments were repeated at least four times at each concentration of TEMPOH(D). Stirring was maintained at a relatively slow rate throughout the duration of each experiment in order to maximize the signal-to-noise ratio in the recorded spectra. Variable-temperature measurements for an Eyring plot were performed as described, with the exception that the reaction vessel was submerged in a cryogenic bath at a desired temperature. Temperatures were invariant throughout the duration of each experiment.

X-ray Crystallography. A purple 0.48 × 0.36 × 0.07 mm^3 crystal plate of **2** was mounted on a glass capillary with oil. Colorless plates of **5** (0.15 × 0.10 × 0.10 mm^3), **6** (0.25 × 0.10 × 0.05 mm^3), and **8** (0.50 × 0.40 × 0.15 mm^3) were each mounted on a glass capillary with oil. A red needle of **7**, measuring 0.15 × 0.05 × 0.05 mm^3, was mounted on a glass capillary with oil. Data were collected for all five compounds on a Bruker APEX II single-crystal X-ray diffractometer at −143 °C for **2** and at −173 °C for **5**−**8**. For **2**, the crystal-to-detector distance was 43.5 mm and the exposure time was 60 s deg^{-1} for all sets. The crystal-to-detector distance for **8** was 40 mm and the exposure time was 20 s deg^{-1} for all sets. The crystal-to-detector distance for **5** and **7** was 40 mm and the exposure time was 10 s deg^{-1} for all sets. The scan width for **2** was 1.0°. The scan width for **5**−**8** was 0.5°. Data collection for **2** was 99.0% complete to 25.68° and 99.0% complete to 25° in ϑ. Data collection for **5** was 99.1% complete to 25.0° in ϑ. Data collection for **6** was 100% complete to 25.0° in ϑ. Data collection for **7** was 96.6% complete to 25.35° in ϑ. Data collection for **8** was 99.5% complete to 28.48° in ϑ. A total of 74378 partial and complete reflections for **2** were collected covering the indices h = −15 to +15, k = −20 to +20, and l = −44 to +44. A total of 7279 reflections were symmetry-independent, and R_{int} = 0.0971 indicated that the data were of less than average quality (0.07). Indexing and unit cell refinement indicated an orthorhombic P lattice. The space group for **2** was found to be *Pbca* (No. 61). For **5**, a total of 85796 partial and complete reflections were collected covering the indices h = −41 to +41, k = −18 to +18, and l = −16 to +16. A total of 6622 reflections were symmetry-independent, and R_{int} = 0.0361 indicated that the data for **5** were good (0.07 average quality). Indexing and unit cell refinement indicated a monoclinic C lattice with the space group $C2/c$ (No. 15). One PF_6^- molecule was found disordered over two positions, each with 50% occupancy. For **6**, 4905 reflections were symmetry-independent and R_{int} = 0.0195 indicated that the data were good (average quality 0.07). Indexing and unit cell refinement indicated a monoclinic P lattice. The space group for **6** was found to be $P2_1/c$ (No. 14). A total of 106880 partial and complete reflections were collected covering the indices h = −11 to +11, k = −22 to +22, and l = −29 to +29. A total of 7668 reflections were symmetry-independent, and R_{int} = 0.0313 indicated that the data for **6** were good (0.07 average quality). Indexing and unit cell refinement indicated a monoclinic P lattice with the space group $P2_1/n$ (No. 14). The PF_6^- and MeCN molecules are each slightly disordered in structure **6**. For **7**, a total of 26870 partial and complete reflections were collected covering the indices h = −16 to +16, k = −9 to +10, and l = −19 to

dx.doi.org/10.1021/ic401234t | *Inorg. Chem.* 2013, 52, 12383−12393

+19. A total of 1868 reflections were symmetry-independent, and R_{int} = 0.0792 indicated that the data for **7** were of average quality (0.07 average quality). Indexing and unit cell refinement indicated an orthorhombic *P* lattice with the space group *Pnma* (No. 62). The structure of **7** exhibits disorder across a mirror symmetry plane through the Mn ion, S atom, and imine N atom. The PF_6^- molecule is heavily disordered with two superimposed geometries at 0.66:0.34 occupancies. A total of 67058 (merged) reflections for **8** were collected covering the indices h = −11 to +11, k = −22 to +22, and l = −18 to +18. A total of 4905 reflections were symmetry-independent, and R_{int} = 0.0195 indicated that the data were good (average quality 0.07). Indexing and unit cell refinement indicated a monoclinic *P* lattice. The space group for **8** was found to be $P2_1/c$ (No. 14).

Data for **2** (Table 1) were integrated and scaled using *hkl*-SCALEPACK. Solution by direct methods (*SIR97*) produced a complete heavy-atom phasing model, consistent with the proposed structure. All non-H atoms were refined anisotropically by full-matrix least squares. All H atoms were located using a riding model. Data for **5**−**8** were integrated and scaled using *SAINT* and *SADABS* within the *APEX2* software package by Bruker. Solution by direct methods (*SHELXS* and *SIR97*)[25] produced a complete heavy-atom phasing model for each, consistent with the proposed structure. The structures were each completed by difference Fourier synthesis with *SHELXL97*.[26,27] Scattering factors are from Waasmair and Kirfel.[28] H atoms were placed in geometrically idealized positions and constrained to ride on their parent atoms with C−H distances in the range of 0.95−1.00 Å. Isotropic thermal parameters U_{eq} were fixed such that they were 1.2U_{eq} of their parent atom U_{eq} for CH groups and 1.5U_{eq} of their parent atom U_{eq} in the case of methyl groups. All non-H atoms were refined anisotropically by full-matrix least squares. For **7**, the structure exhibited disorder across a crystallographic mirror symmetry plane containing the Mn, S, and N(1) atoms. For **8**, a cocrystallized water molecule was found to be disordered over two different hydrogen geometries, one in which there is hydrogen bonding to the F(2) atom of PF_6^- and a second in which there is hydrogen bonding to a thiolate sulfur of an adjacent molecule as well as another fluoride of PF_6^-.

RESULTS AND DISCUSSION

Synthesis and Structure of Monooxo-Bridged 2. The addition of O_2 to coordinatively unsaturated **1**[24] in MeCN affords a rare example of an unsupported monooxo-bridged manganese(III) dimer **2**. Single crystals of **2** suitable for X-ray diffraction studies were obtained via crystallization from MeCN/Et_2O. As shown in the ORTEP diagram of Figure 2,

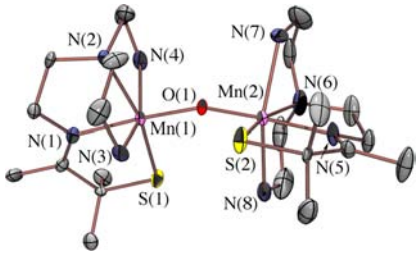

Figure 2. ORTEP of monooxo-bridged **2**, with H atoms and counteranions omitted for clarity.

each Mn center of **2** is six- coordinate and ligated by an oxo trans to an imine nitrogen and cis to a thiolate sulfur. Although there are numerous examples of μ-carboxylate-μ-oxo- and dioxomanganese(III) dimers,[29−33] there are significantly fewer examples containing a single, unsupported oxo bridge.[34−37] Thiolate-ligated monooxo-bridged dimanganese complexes are even more rare and include pyridine and quinoline derivatives of **2**, $[Mn^{III}(S^{Me2}N_4(6\text{-Me-DPEN}))]_2(\mu\text{-O})(PF_6)_2\cdot 2MeCN$ (**3**),[35] and $[Mn^{III}(S^{Me2}N_4(2\text{-QuinoEN}))]_2(\mu\text{-O})(PF_6)_2$ (**4**).[35] The Mn−S(1) bond length of oxo-bridged **2** is 0.13 Å shorter than that of reduced **1**[24] (Table 2) and comparable to those of N-heterocyclic amine-ligated oxo-bridged **3** and **4**,[35] consistent with an increase in the oxidation state from Mn^{II} to Mn^{III}. The trans Mn−N(3) and Mn−N(4) bonds in **2** are elongated somewhat relative to Mn−N(2), reflecting a Jahn−Teller-like distortion; however, this distortion is significantly less than that seen with the more sterically encumbered complexes **3** and **4**.[35] No intermediates are observed in the reaction between **1** and O_2, even at temperatures as low as −80 °C. This is in contrast to the more sterically encumbered, π-accepting N-heterocyclic amine compound $[Mn^{II}(S^{Me2}N_4(6\text{-Me-DPEN})]^+$, which forms observable Mn−O_2 and peroxo intermediates in its low-temperature reaction with O_2.[38] The Mn−O(1) bond to the bridging oxo is slightly longer in **2** (1.791 Å; average) relative to **3** [1.7602(4) Å] and **4** [1.7599(6) Å], indicating that it has slightly less double-bond character. Consistent with this, the Mn−O−Mn bridging angle of **2** is fairly bent (158.75°), and the S(1)N(1)N(2)O(1)Mn(1) and S(2)N(5)N(6)O(1)Mn(2) planes (Figure S-1 in the Supporting Information, SI) are close to orthogonal (dihedral angle = 69.1°). The bent bridging Mn−O−Mn angle is in contrast to the majority of reported monooxo-bridged dimanganese complexes,[36] including **3** (180°) and **4** [172.3(2)°],[35] which are approximately linear. The only example of a more acute Mn−O−Mn angle [146.15(11)°] is in the unstable oxo-bridged $\{[Mn^{III}(S^{Me2}N_4(6\text{-Me-DPPN}))]_2\text{-}(\mu\text{-O})\}^{2+}$.[35] A possible explanation for the acute angle is that, in the absence of steric repulsion between the *gem*-dimethyl groups adjacent to the sulfur and the amine ligand, the highly covalent π-donor thiolate ligand would compete more effectively than the oxo for π overlap with the Mn d orbitals, resulting in less Mn═O−Mn ↔ Mn−O═Mn double-bond character. This would free up a lone pair on the oxo, causing the Mn−O−Mn angle to bend, creating a more basic oxo. The thiolate ligand would also contribute to an increased basicity. The iron analogue of **2**, $\{[Fe^{III}(S^{Me2}N_4(tren))]_2\text{-}(\mu\text{-O})\}^{2+}$,[39] has been shown to readily react with proton donors HA and has a Fe−O−Fe angle [155.3(5)°] similar to that of **2**.

Proton-Induced Cleavage of the μ-Oxo Dimer in MeCN. The μ-oxo bridge of **2** is readily cleaved with proton donors ROH (PhOH, ^{p}NO_2PhOH, MeOH, and H_2O) in MeCN to afford a series (Figure 3) of new Mn^{III}OR complexes, $[Mn^{III}(S^{Me2}N_4(tren))(OR)]^+$ [R = ^{p}NO_2Ph (**5**), Ph (**6**), Me (**7**), or OH^+ (**8**)] including a rare example[40,41] of a monomeric Mn^{III}OH compound. Compound **8** is unusual in that it is monomeric (vide infra) despite the lack of steric bulk. The only other reported examples of monomeric Mn^{III}OH compounds contain bulky substituents designed to protect the hydroxide.[40,41] The monomeric structure of each RO-bound derivative described herein, including hydroxide-bound **8**, was verified by X-ray crystallography (vide infra). Preliminary evidence to suggest that ROH reacts with **2** involved monitoring of the reaction by electronic absorption spectroscopy. A color change, from purple to red, was observed, and peaks grew in at 500 and 411 nm (H_2O; Figures 4 and S-2 in the SI), 439 nm (MeOH; Figures S-3 and S-4 in the SI), 505 nm (PhOH; Figure S-5 in the SI), or 460 nm (^{p}NO_2PhOH; Figures S-6 and S-7 in the SI). These spectral changes involved either a blue shift, or the complete disappearance, of the 520 nm band associated with binuclear **2** (Figure S-8 in the SI). The number of equivalents of proton donor required for complete conversion was found to

dx.doi.org/10.1021/ic401234t | *Inorg. Chem.* 2013, 52, 12383−12393

Table 2. Selected Bond Distances (Å) and Bond Angles (deg) for 1,[24] 2, 3,[35] 4,[35] 5, 6, 7, and 8

	1	2	3	4	5	6	7	8
Mn−S(1)	2.412(3)	2.286(2)	2.2767(7)	2.292(1)	2.2578(8)	2.2675(3)	2.2937(14)	2.2840(4)
Mn−N(1)	2.166(8)	2.017(6)	1.999(3)	2.010(3)	1.999(2)	2.0043(10)	2.018(4)	2.0133(9)
Mn−N(2)	2.334(8)	2.172(7)	2.151(2)	2.130(3)	2.148(2)	2.1474(10)	2.176(5)	2.1634(9)
Mn−N(3)	2.201(8)	2.351(8)	2.581(2)	2.543(3)	2.288(2)	2.3152(11)	2.295(4)	2.275(1)
Mn−N(4)	2.198(8)	2.280(6)	2.501(2)	2.370(3)	2.300(2)	2.3173(10)	2.295(4)[a]	2.3322(9)
Mn(1)−O(1)	N/A	1.783(5)	1.7602(4)	1.7599(6)	1.901(2)[b]	1.8678(8)[c]	1.836(5)[d]	1.8540(8)[e]
Mn(2)−O(1)	N/A	1.799(5)	1.7602(4)[f]	1.7599(6)	N/A	N/A	N/A	N/A
Mn(1)···Mn(2)	N/A	3.521	3.520	3.512	N/A	N/A	N/A	N/A
S(1)−Mn−N(1)	81.9(3)	83.1(2)	82.08(8)	82.60 (8)	83.94(7)	83.26(3)	83.53(12)	83.48(3)
S(1)−Mn−N(2)	158.8(2)	164.6(2)	164.17(7)	163.90(9)	166.11(7)	165.65(3)	166.05(13)	165.40(3)
S(1)−Mn−N(3)	115.0(3)	104.6(2)	106.19(6)	101.40(8)	104.36(7)	98.47(3)	103.42(9)	98.85(3)
S(1)−Mn−N(4)	109.1(2)	102.3(2)	106.84(6)	109.23(8)	103.45(8)	107.23(3)	103.42(9)	106.63(3)
N(1)−Mn−N(3)	125.0(3)	87.1(3)	86.85(6)	94.92(11)	91.19(9)	95.36(4)	90.92(9)	96.12(4)
N(1)−Mn−N(4)	109.5(3)	89.7(3)	92.68(13)	84.75(11)	97.35(9)	87.89(4)	90.92(9)	89.19(3)
N(3)−Mn−N(4)	112.2(3)	152.3(3)	146.57(6)	149.03(10)	151.61(10)	154.30(4)	153.1(2)[a]	154.41(3)
S(1)−Mn−O(1)	N/A	96.6 (2)	95.37(2)	99.20(3)	98.38(7)[b]	99.20(3)[c]	98.78(15)[d]	96.88(3)[e]
N(1)−Mn−O(1)	N/A	177.7(3)	177.21(9)	177.02(12)	173.15(9)[b]	171.55(4)[c]	173.2(7)[d]	177.30(4)[e]
Mn−O(1)−Mn	N/A	158.8(3)	180.0	172.3(2)	N/A	N/A	N/A	N/A
Mn−O(1)−C	N/A	N/A	N/A	N/A	136.8(2)[b]	134.25(7)[c]	124.0(9)[d]	N/A

[a]For this structure, N(3) and N(4) are equivalent and related by a crystallographically imposed mirror plane. [b]In this case, O(1) = $^{p}NO_2$-phenoxide oxygen. [c]In this case, O(1) = phenoxide oxygen. [d]In this case, O(1) = methoxide oxygen. [e]In this case, O(1) = hydroxide oxygen. [f]For this structure, the halves of the "dimer" are related by crystallographic symmetry so that Mn(1) = Mn(2).

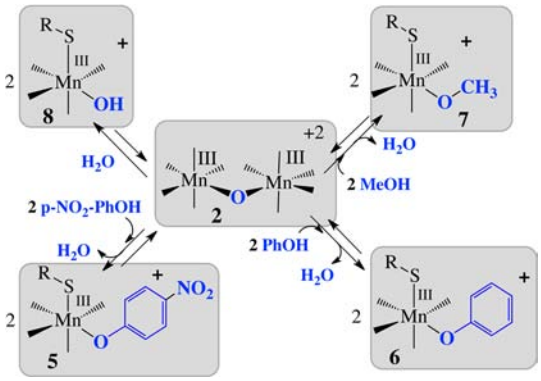

Figure 3. Reaction scheme outlining the observed conversion of oxo-bridged **2** to monomeric *p*-nitrophenoxide-, phenoxide-, methoxide-, and hydroxide-ligated **5**−**8** via the addition of the corresponding ROH in MeCN.

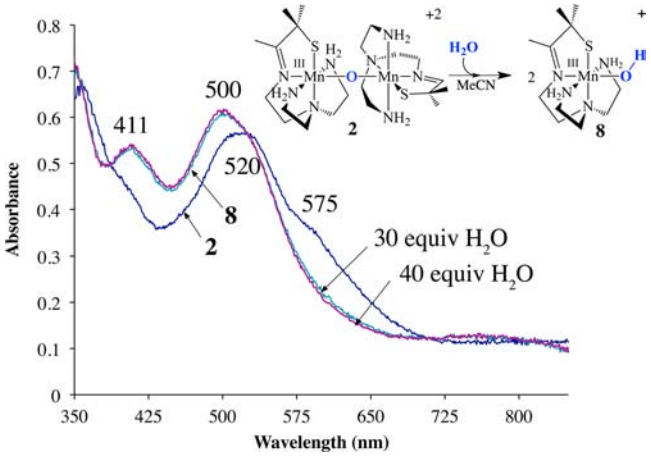

Figure 4. Conversion of oxo-bridged **2** to monomeric hydroxide-ligated **8** via the addition of 0−40 equiv of H_2O in MeCN, as monitored via electronic absorption spectroscopy.

vary with the acidity of the proton donor: $^{p}NO_2PhOH$ (9 equiv; pK_a = 22 in MeCN)[42,43] and PhOH (15 equiv; pK_a = 27.2 in MeCN),[42,43] versus H_2O (40 equiv) and MeOH (75 equiv; pK_a ≫ 33 in MeCN).[42,43] *tert*-Butanol does not react with **2**, setting upper and lower limits to the bridging oxo pK_a in MeCN: pK_a(MeOH) < pK_a(Mn-oxo) < pK_a(^{t}BuOH). No reaction is observed between **2** and NaOPh$^{p}NO_2$, NaOPh, and NaOMe, indicating that these reactions (Figure 3) are proton-dependent. This would be consistent with a mechanism involving the initial protonation of the bridging oxo of **2** to form binuclear μ-hydroxo-bridged $[Mn^{III}(S^{Me2}N_4(tren)]_2(\mu OH)(PF_6)_2$ (**2**-H$^+$). A μ-OH bridge would be weakened relative to an oxo bridge.[44] Alkoxide/phenoxide (RO^-)-induced cleavage of the hydroxo bridge would then afford 1 equiv of $[Mn^{III}(S^{Me2}N_4(tren))(OR)]^+$ [R = $^{p}NO_2Ph$ (**5**), Ph (**6**), or Me (**7**)] and 1 equiv of **8**. The hydroxo-bridged intermediate, **2**-H$^+$, is not observed in any of these reactions (Figure 3), indicating that RO^--induced cleavage of the μ-OH bridge occurs more rapidly than the initial protonation step. Rate-limiting μ-oxo protonation would be consistent with Norton's previously reported observations.[45] It is also possible that the weakened μ-OH bridge cleaves prior to RO^- attack to afford **8** and a solvent-bound Mn^{III}NCMe species, which then reacts with the first 1 equiv of RO^- released during the bridge protonation step to afford **5**, **6**, or **7**. The addition of a second equiv of ROH to the 1 equiv of **8** formed following rupture of the μ-OH bridge would afford a second 1 equiv of **5**−**7** and H_2O. Consistent with this, phenoxy and methoxy derivatives **5**−**7** can also be generated via the addition of ROH to hydroxo-bound **8** (Scheme S-1 and Figures S-9−S-11 in the SI). A total of 2 equiv of **8** is formed directly via the addition of H_2O to **2** in MeCN. Again, the number of equivalents of ROH required for complete conversion **8** → **5** (8 equiv), **6** (15 equiv), or **7** (120 equiv) was found to be dependent on the relative acidity

dx.doi.org/10.1021/ic401234t | *Inorg. Chem.* 2013, 52, 12383−12393

Scheme 1

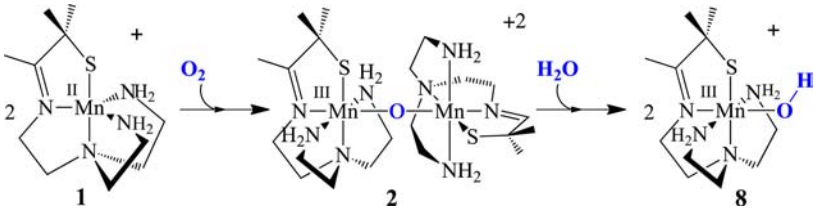

of $MnOH_2$ versus ROH. The ability of proton donors as basic as MeOH to cleave the oxo bridge of **2** contrasts with the lack of reactivity between pyridine- and quinoline-ligated **3** and **4**[35] and H_2O or MeOH. This likely reflects the reduced basicity of the O atom of **3** and **4** relative to that of primary amine-ligated **2** due to the π-acceptor properties of the pyridine and quinoline ligands, elongated Mn···N(3,4) bonds, and more linear Mn−O−Mn bridge. The former would create a more Lewis acidic metal center. Although it is ligated by σ-donating primary amines, the μ-oxo bridge of $\{[Fe^{III}(S^{Me2}N_4(tren)](\mu\text{-}O)[Fe^{III}(S^{Me2}N_4(tren)]\}^{2+}$ is only cleaved with more acidic proton donors (HCl, $LutNH^+$, TfOH, and HOAc). This reflects the increased metal-ion Lewis acidity of Fe^{3+} relative to Mn^{3+}, which decreases the basicity of the O atom. The bridging oxo of pyridine- and carboxamido-ligated $[(Mn^{III}(PaPy_3))_2(\mu\text{-}O)]^{2+}$ reported by Mascharak and co-workers is also readily protonated by proton donors as basic as MeOH to afford the corresponding monomeric complexes $[Mn^{III}(PaPy_3)(L)]^+$ (L = MeO^-, PhO^-, AcO^-, BzO^-).[46] An L = HO^- derivative was not reported for this series. Hydroxo-bound **8** is most readily isolated via aerobic oxidation of **1** in aqueous solutions as described below.

Synthesis of Hydroxo-Bound 8 in Water. Aerobic oxidation of **1** in H_2O cleanly affords **8** in high yields (99%). Hydroxo-bound **8** can also be generated by dissolving preisolated crystalline samples of μ-oxo **2** in H_2O, indicating that oxo-bridged **2** forms en route to hydroxo-bound **8** (Scheme 1). By varying the aqueous pH and monitoring changes to the electronic absorption spectrum, we determined that the Mn^{III}−O−Mn^{III} bridge of **2** is readily cleaved in solutions as basic as pH 10. This observation implies that the bridging O atom of **2** is fairly basic ($pK_a \geq 10$). Our inability to observe hydroxo-bridged $\{[Mn^{III}(S^{Me2}N_4(tren))]_2(\mu\text{-}OH)\}^{2+}$ (**2**-H^+), which is presumed to be an intermediate in the conversion of **2** to **8** did not allow us to more quantitatively determine the pK_a of the O atom of **2**. Another factor is the limited aqueous solution stability of **8** at extremely basic pHs. Optimum stability (on the order of hours) is observed in the pH range $6 \leq pH \leq 8.5$. At pH > 10.5, **8** is short-lived and converts to a black precipitate, presumably Mn_2O_3, or possibly MnO_2 (if disproportionation is involved), within minutes.

Comparison of the Crystallographic Structures of Thiolate-Ligated Mn^{III}OR Compounds. The structures of the four Mn^{III}OR compounds described in this study, **5**−**8**, were determined by X-ray crystallography. ORTEP diagrams of the more stable complexes are shown in Figure 5 and the slightly less stable, more reactive complexes in Figure 6. All four compounds are mononuclear. In particular, mononuclear Mn^{III}OH hydroxide complexes are extremely rare.[40,47−50] The Mn^{III} ion in all four compounds is pseudooctahedral and contains either an $^pNO_2PhO^-$ (**5**), PhO^- (**6**), MeO^- (**7**), or OH^- (**8**) trans to an imine nitrogen [N(1)] and cis to a thiolate sulfur. The metrical parameters are compared in Table 2. A

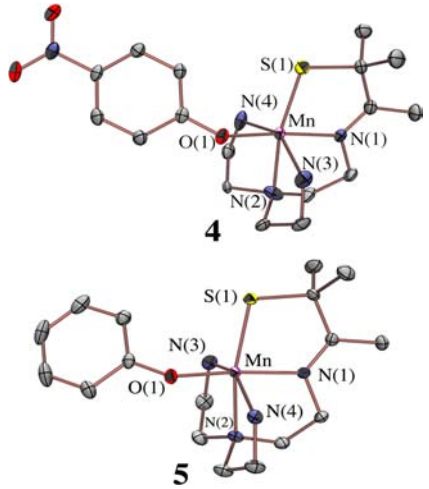

Figure 5. ORTEP of **6** and **5**, with H atoms, counteranions, and solvents of crystallization omitted for clarity.

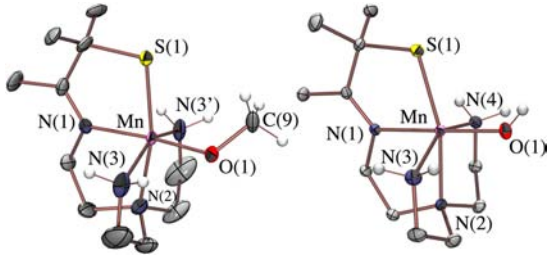

Figure 6. ORTEP of **7** and **8**, with H atoms omitted for clarity.

comparison of the Mn−S(1) bond lengths in **5**−**8** with that of reduced **1**[24] and oxo-bridged **2**−**4** indicates that the Mn ions are clearly oxidized in **5**−**8** relative to **1**. Although much less exaggerated than that with sterically encumbered oxo-bridged **3** and **4**, elongation of the trans Mn−N(3) and Mn−N(4) bonds is observed in **5**−**8** relative to reduced **1**. This would also be consistent with each compound containing a Mn^{3+} ion with an odd antibonding electron. With the exception of hydroxide-bound **8** (vide infra), the Mn−O(1) distance decreases [from 1.901(2) Å in **5** to 1.836(5) Å in **7**] as the electron-withdrawing ability (via resonance) of the R group decreases. Resonance between the oxygen lone pairs and phenyl rings of **5** and **6** removes the negative charge from the oxygen and ties up one of the lone pairs that would otherwise be available to interact with protons. This would be expected to influence reactions involving proton addition to the coordinated oxygen (vide infra). The short Mn−O(1) bond distances and Mn−O(1)−C bond angles near 120° (Table 2) indicate that the oxygen O(1) in these structures is sp^2-hybridized and involved in π bonding to the metal, consistent with some Mn═OR double-bond character. The Mn−O(1)−C angle increases in the order **7** < **6**

dx.doi.org/10.1021/ic401234t | Inorg. Chem. 2013, 52, 12383−12393

< **5**, indicating that an oxygen lone pair is partially involved in resonance with the aromatic ring in structures **5** and **6** as well resulting in partial O═C^{phenyl} character. The short aromatic C−O(1) bond distance [1.321(3) Å in **5** and 1.3404(15) Å in **6** vs the typical C^{aromatic}−O bond distance of 1.362 Å in free PhOH] would be consistent with this. In contrast, the methoxide C−O bond length in **7** [1.413(13) Å] matches that of free MeOH (1.413 Å). The Mn−O(1) hydroxide distance [1.8540(8) Å] in **8** is longer than expected, based on the pK_a of H_2O relative to the other members of the series. This is because the hydroxide ion is hydrogen-bonded to a cocrystallized H_2O molecule [O(1)···H(2G)O(2)H = 1.890 Å; O(1)···O(2) = 2.660 Å] in the solid state. There is also a weak intramolecular hydrogen bond between one of the primary amine N(3,4)H_2 protons and the bound hydroxide oxygen O(1) [N(3)H···O(1) = 2.730 Å] in **8**. This effect is modified somewhat by an intermolecular hydrogen bond of the opposite nature (i.e., one which pushes the electron density back onto the hydroxide oxygen) between the hydroxide proton and thiolate sulfur of a neighboring molecule [O(1)H···S(1) = 2.466 Å; Figure S-17 in the SI]. Weak intramolecular hydrogen bonds are also observed between the alkoxide [N(3)H···O(1)= 2.632 Å in **7**] and phenoxide [N(4)H···O(1) = 2.796 Å in **5**; N(4)H···O(1) = 2.682 Å in **6**] O atoms and primary amine N−H protons. Again with the exception of hydroxide-bound **8**, these intramolecular hydrogen-bond distances roughly correlate with ROH pK_a. There is an inverse correlation between the Mn^{III}−SR and Mn−OR bond lengths (Figure S-18 in the SI): the Mn−S(1) bond length increases as the Mn−O(1) bond length decreases (Table 2). This reflects the flexible nature of the Mn−SR bond and its ability to compensate for changes in the electron density at the metal ion.[51] It also reflects the fact that both the thiolate and alkoxide are competing for overlap with the same π−d orbital. An increased Mn^{III}−SR bond covalency might be responsible in part for the increased stability of phenoxide-ligated **5** and **6** versus methoxide- and hydroxide-ligated **7** and **8**.

Solution Properties of [Mn^{III}(S^{Me2}N$_4$(tren))(OR)]$^+$ [R = ^{p}NO$_2$Ph (5), Ph (6), Me (7), and H (8)] Relevant to the Reactivity. The most stable thiolate-ligated Mn^{III}OR derivatives, **5** and **6**, are derived from the more acidic alcohols PhOH (pK_a= 27.2 in MeCN)[42,43] and ^{p}NO$_2$PhOH (pK_a = 22 in MeCN).[42,43] The more reactive (vide infra), and consequently somewhat less stable derivatives **7** and **8** are derived from the less acidic proton donors MeOH and H_2O (pK_a ≫ 32 in MeCN).[42,43] The stability was assessed based on changes to the electronic absorption spectrum. Ambient temperature solutions of **7** [$\tau_{1/2}$(MeCN, 298 K) = 1.9 h] and **8** [$\tau_{1/2}$(H_2O, 298 K) = 3.8 h] were found to decay in approximately half a day, whereas those of **5** and **6** showed no signs of decay even after 1 week. In the solid state, compounds **7** and **8** were found to be more robust and were stored in a −80 °C freezer. For solution studies [i.e., quantitative electronic absorption spectroscopy (vide supra), kinetics (vide infra), and electrochemistry], fresh samples of **7** and **8** were prepared in every case. Cyclic voltammograms of **5**−**8** (Figures S-13−S-17 in the SI) display irreversible waves indicating that, like our previously reported compounds [M^{III}(S^{Me2}N$_4$(tren))(L)]$^+$ (M = Co, Fe),[24,52] the six-coordinate structure converts to a five-coordinate structure upon reduction. This has been attributed to the π-donating properties of the thiolate, which decrease the Lewis acidity of the metal center, especially when it is in a lower oxidation state.[53] The cathodic peak potentials for **5**−**8** (E_{pc}; Table 3) were found to be reproducible to within ±10 mV and become increasingly negative as the electron-withdrawing ability of the R group (via resonance) decreases. Given their potentials, none of these compounds would be expected to behave as a strong oxidant. In fact, hydroxide- and methoxide-bound **8** and **7** have the lowest (i.e., most negative) Mn$^{III/II}$ potential within the series and should therefore be the weakest oxidants, and yet they turn out to be the most reactive and capable of abstracting H atoms (vide infra), suggesting that something other than the redox potential is governing their reactivity. Phenoxide-ligated **5** and **6** were found to be unreactive. The reactivity of **8** was explored in both H_2O and MeCN, and that of **7** was explored only in MeCN.

Table 3. Redox Properties, Proton Affinity, and O−H BDFE of Mn$^{III/II}$O(H)R Compounds in MeCN or H_2O

	$E_{p,c}$ (mV vs $Fc^{+/0}$) in MeCN	estimated pK_a of Mn^{II}O(H)R in MeCN	BDFE in MeCN (kcal mol^{-1})	BDFE in H_2O (kcal mol^{-1})
MnOPh^{p}NO$_2$ (**5**)	−220	<12.2	N/A	N/A
MnOPh (**6**)	−300	<13.5	N/A	N/A
MnOMe (**7**)	−450	≥16.2	N/A	N/A
MnOH (**8**)	−600	21.2	70.1	74.0(5)

PCET to 8 in Water. Of the four Mn^{III}OR complexes **5**−**8**, only **8** is stable in water. This water solubility provides a wealth of thermodynamic information (vide infra), in addition to facilitating aerobic oxidation catalysis under environmentally friendly conditions (vide infra). The redox potential of **8** in H_2O is pH-dependent (Figure 7 and Table S-0 in the SI),

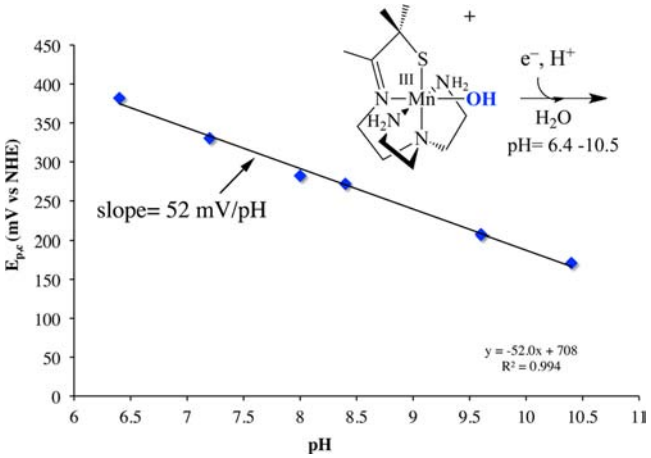

Figure 7. Pourbaix diagram for **2** in an aqueous solution. The pH was adjusted using dilute aqueous solutions of either HBF_4 or NH_4OH, and the cathodic peak potentials were measured at 298 K in H_2O with 0.1 M $KClO_4$ as the supporting electrolyte and a glassy carbon electrode.

indicating that PCET is involved. The slope of the aqueous Pourbaix diagram of Figure 7 (52 mV pH^{-1}) is close to that expected (59 mV pH^{-1}) for ideal Nernstian behavior and is indicative of the transfer of a single proton with each electron. The significance of this is that the reverse process, i.e., Mn^{II}H$_2$O → Mn^{III}OH + H$^+$ + e$^-$, is involved in photosynthetic water splitting.[54−56] The pH range examined (Figure 7) reflects the stability range of the manganese(III) hydroxo compound **8**. The low aqueous redox potentials [380 mV ≥ $E_{p,c}$(**8**) ≥ 150 mV vs NHE] over the pH range examined (6.2 ≤ pH ≤ 10.5;

dx.doi.org/10.1021/ic401234t | Inorg. Chem. 2013, 52, 12383−12393

Figure 7) indicate that **8** is a very mild oxidant in water. Using the aqueous Pourbaix diagram for **8** (Figure 7), one can directly calculate the aqueous O−H bond dissociation free energy (BDFE) for the product of PCET, $[Mn^{II}(S^{Me2}N_4(tren))(H_2O)]^+$ (**9**; Scheme 2), using eq 1, where E_{pH} is the redox

Scheme 2

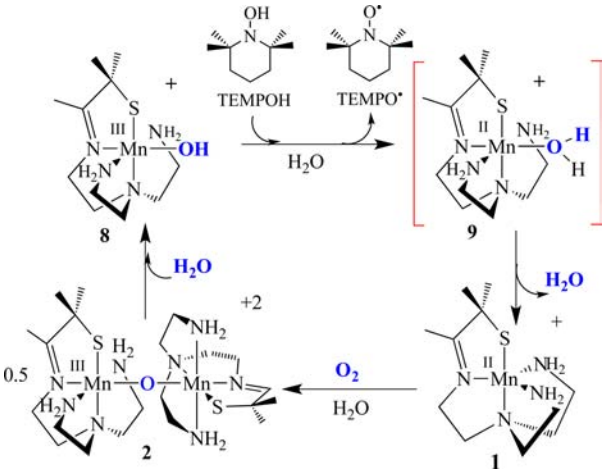

potential of **8** at a given pH, and the constant 57.6 kcal mol^{-1} is the solvent-dependent energy of formation and solvation ($C_{G,sol}$) of H$^•$ in H_2O.[1]

$$\text{BDFE}[Mn^{II}(HOH)] = 23.06E_{pH} + 1.37\text{pH} + 57.6 \text{ kcal mol}^{-1} \quad (1)$$

This equation represents a modified form[1] of the Bordwell equation,[8,9] for use specifically in aqueous solution reactions. The use of cathodic peak potentials, $E_{p,c}$, in place of $E_{1/2}$, has been previously shown to introduce essentially no error in BDFE calculations for species involved in irreversible redox reactions.[1,9] The redox potential used in eq 1 is referenced to NHE according to the convention for aqueous BDFE calculations.[1] The relationship between the cathodic peak potential and pH ($E_{pH} = E^\circ_{pH\,0} - (0.052\text{pH}$; $E^\circ_{pH\,0} = +0.708$ V), obtained from the least-squares fit to the data of Figure 7, provided E_{pH} values for this calculation. On the basis of this calculation, the O−H BDFE for **9** was determined to be 74.0 ± 0.5 kcal mol^{-1} (Figure 8 and Table 3). This O−H bond strength is significantly lower than that of free H_2O (119 kcal mol^{-1}), demonstrating that water coordination to Mn^{II}

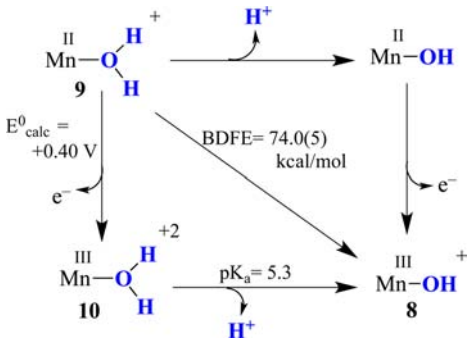

Figure 8. Thermochemical cycle for **8**-promoted PCET reactions in an aqueous solution. Potentials are referenced to NHE.

significantly activates the O−H bond, a property that is relevant to water splitting in photosynthesis. Using the Bordwell equation (2)[8,9] (with $9C_{G,H2O}$ = 57.6 kcal mol^{-1} for H_2O), the experimentally determined pK_a = 5.3 of **9**, and the BDFE obtained from the Pourbaix data (74.0 kcal mol^{-1}), the formal potential for the $[Mn^{III}OH_2]^{2+}$ (**10**)/**9** couple (+0.40 V vs NHE; Figure 8) was calculated.

$$\text{BDFE}[M^{II}(HOH)] = 23.06E^\circ(M^{III}/M^{II}) + 1.37\text{p}K_a + C_{G,sol} \quad (2)$$

The proton dissociation constant for **9** was determined to be pK_a = 5.3 via HOTf + **8** titration experiments (Figure S-20 in the SI). Because of their instability in H_2O, Pourbaix diagrams were not obtained for the methoxide and phenoxide derivatives $Mn^{III}OMe$ (**7**), $Mn^{III}OPh$ (**6**), and $Mn^{III}OPh^pNO_2$ (**5**), making it impossible to calculate the O−H BDFE of the corresponding reduced protonated derivatives of these complexes. The PCET properties of **8** suggested that it would be capable of promoting PCET-type reactions involving substrates with weaker X−H bonds.

Aqueous Reactions between 8 and TEMPOH. Reactions between hydroxide-bound **8** and TEMPOH in H_2O were monitored by electronic absorption spectroscopy (Figure 9)

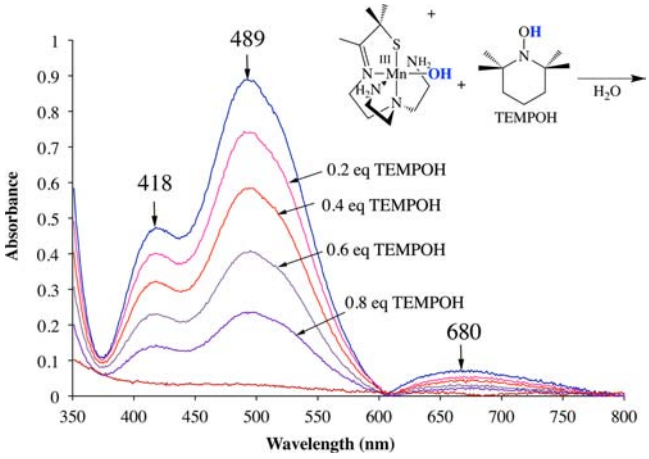

Figure 9. Anaerobic reaction between **8** and 0.2 equiv aliquots of TEMPOH in H_2O at 298 K, showing that 1.0 equiv of TEMPOH is required to convert **8** to five-coordinate **1**, presumably via an unobserved reduced water-bound intermediate **9**.

and shown to involve the disappearance of visible bands at 418 and 489 nm to afford a featureless UV/vis spectrum characteristic of **1**[24] (Scheme 2). Titration experiments show that a clean 1:1 (**8**/TEMPOH) stoichiometric reaction is involved.

Kinetic data (vide infra) suggest that the reaction involves an unobserved reduced six-coordinate intermediate **9** (Scheme 2), which was shown by cyclic voltammetry (vide supra, Figure S-17 in the SI) to be unstable on the time scale of these experiments. This reactivity would be consistent with the relative O−H bond strengths of **9** (BDFE = 74 kcal mol^{-1}) versus that of TEMPOH (BDFE = 71 kcal mol^{-1}),[1] in H_2O. Quantitative conversion back to **8** (Figure S-21 in the SI) is observed upon the addition of O_2 to the TEMPOH-reduced product (Scheme 2). Given that oxo-bridged **2** forms upon O_2 addition to **1** and converts to hydroxo-bound **8** in H_2O, it is likely that oxo-bridged **2** forms as an intermediate en route to **8**

dx.doi.org/10.1021/ic401234t | Inorg. Chem. 2013, 52, 12383−12393

(Scheme 2). At least 10 turnovers (likely more) can be achieved without significant degradation of the "catalyst" **8** (Figure S-22 in the SI). The net reaction promoted by **8** (Scheme 2), i.e., O_2-promoted TEMPOH oxidation in H_2O at ambient temperatures, is thus done under environmentally friendly ("green") conditions. No reaction is observed between hydroxide-bound **8** and 1,4-cyclohexadiene, 9,10-dihydroanthracene, or toluene. On the basis of their self-exchange rate constants,[10] these substrates would be expected to react at a rate that is slower than the decomposition rate of **8** [$\tau_{1/2}(H_2O$, 298 K) = 3.8 h].

Estimated Thermodynamic Ability of 8 To Abstract H Atoms in MeCN. Complex **8** is the only known $Mn^{III}OH$ complex for which thermodynamic data, predictive of the H-atom-abstraction capability, are reported in water. This unfortunately precludes a comparison between the O−H BDFE of the corresponding reduced complex **9** and other similar systems for which data are reported in MeCN[48] or acetone/H_2O (4:1).[16] By determination of the thermodynamic parameters for **9** in organic solvents such as MeCN, comparisons could then be made. Although a cathodic peak potential could be obtained for **8** in MeCN (Table 3), the "pK_a" of protonated **10** (Figure 8) in MeCN could not be experimentally determined, because MeCN displaces the H_2O ligand. This ultimately prevented an experimental determination of the O−H BDFE for **9** (Scheme 2) in MeCN. A crude approximation of this O−H BDFE [BDFE(**9**)] can be made, however, if we assume that the solvation energies of **8** and **9** are the same. If this is assumed, then the difference between the O−H BDFE for **9** in MeCN versus H_2O is equal to the difference between the free energy of solvation for $H^•$ in MeCN (5.12 kcal mol^{-1}) and H_2O (8.98 kcal mol^{-1}), affording a BDFE for **9** in MeCN of 70.1 kcal mol^{-1} (Table 3). This estimated BDFE would suggest that **8** should be capable of abstracting a H atom from TEMPOH (O−H BDFE = 66.5 kcal mol^{-1} in MeCN)[1] in MeCN, consistent with what is observed.

HAT Reactivity of 8 and 7 in MeCN. As anticipated, on the basis of the thermodynamic discussion above, hydroxide-bound **8** reacts quantitatively with TEMPOH in MeCN at 298 K. This was determined by monitoring the reaction between **8** and TEMPOH (0.2 equiv aliquots) in MeCN using electronic absorption spectroscopy (Figure S-23 in the SI). Methoxide-bound **7** was also found to react quantitatively with TEMPOH in MeCN (Figure S-24 in the SI). A total of 1 equiv of TEMPOH was required for the complete disappearance of **7** (Figure S-24 in the SI) or **8** (Figure S-23 in the SI), indicating that a clean 1:1 stoichiometric reaction is involved. The initial products expected in these reactions $[Mn^{II}(S^{Me2}N_4(tren))(ROH)]^+$ (R = H, Me) are not observed, consistent with the electrochemical data (vide supra; Figures S-13 and S-14 in the SI), which demonstrates that these six-coordinate reduced species are unstable[52,57] on the time scale of these experiments. Phenoxide-bound **5** and **6** show no reaction with TEMPOH, even when excess substrate is added and the reaction mixture is monitored for prolonged periods under anaerobic conditions (~24 h). This would imply that the O−H BDFE of $[Mn^{II}(S^{Me2}N_4(tren))(ROH)]^+$ (R = Ph, Ph^pNO_2) is less than 66.5 kcal mol^{-1}, the O−H bond BDFE of TEMPOH.

Kinetics of the Reaction between 8 and 7 and TEMPOH in MeCN. Oxidation of TEMPOH by **8** is reasonably fast (Figure S-25 in the SI) in MeCN, with a second-order rate constant of k(298 K) = 2.1 × 10^3 M^{-1} s^{-1} (Figure S-26 in the SI), k_H/k_D = 3.1 (Figure 10), and activation

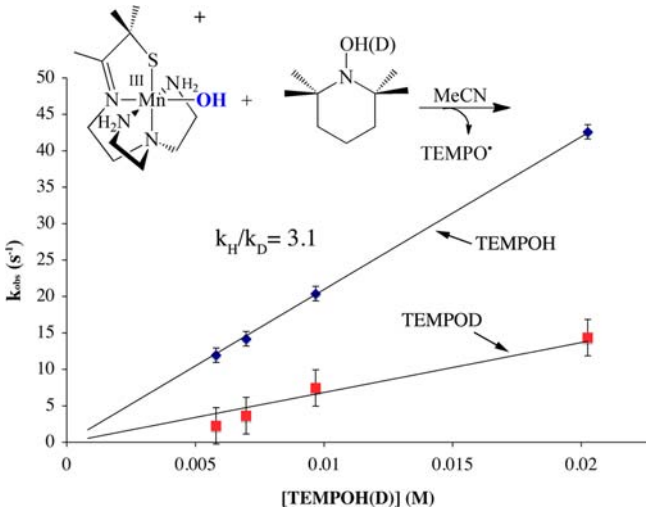

Figure 10. Kinetic isotope effect (k_H/k_D) for the reaction between **8** (0.5 mM) and TEMPOH(D) in MeCN at 298 K.

parameters of $\Delta H^‡$ = 8.2 kcal mol^{-1} and $\Delta S^‡$ = −25.5 eu (Figure S-27 in the SI). TEMPOH oxidation by **7** is roughly an order of magnitude slower than **8**, with a second-order rate constant of k(298 K) = 3.6 × 10^2 M^{-1} s^{-1} (Figure S-28 in the SI), an ambient temperature k_H/k_D = 2.1 (Figure S-28 in the SI), and activation parameters of $\Delta H^‡$ = 8.3 kcal mol^{-1} and $\Delta S^‡$ = −29 eu (Figure S-29 in the SI). The observed deuterium isotope effects for the reaction between **7** and **8** and TEMPOH in MeCN, coupled with the high oxidation potential (E = +710 mV vs $FeCp_2/FeCp_2^+$) and pK_a (pK_a = 41) of TEMPOH,[1] would be *consistent with a mechanism involving concerted HAT*, as opposed to sequential H^+ followed by e^- transfer or vice versa.

Factors Responsible for the Ability of 8 and 7 to Abstract H Atoms. According to the Bordwell equation (eq 2),[1,8−12] in relation to thermodynamic cycles such as that of Figure 8, the two factors that determine the driving force for HAT reactions are the redox potential of the oxidant (e.g., $Mn^{III}OR$) and the pK_a value of the reduced protonated product [e.g., $Mn^{II}O(R)H$]. If one compares the cathodic peak potentials ($E_{p,c}$) of **5**−**8** in MeCN (Table 3), one would not expect any of these complexes to be capable of oxidizing TEMPOH, and on the basis of their $E_{p,c}$ values, one would expect the phenoxide complexes **5** and **6** to be better oxidants than either the methoxide or hydroxide complexes **7** and **8**. This is in contrast to the observed reactivity, however, *suggesting that the trend in pK_a values opposes that of $E_{p,c}$ for these compounds*. The pK_a values required in order to abstract a H atom from TEMPOH in MeCN at a given potential are illustrated in Figure 11. These were calculated using the Bordwell equation (2), with potentials referenced relative to Cp_2Fc^+/Cp_2Fc according to the convention.[1] From this, one can see that even with a cathodic peak potential as low as −600 mV (vs Cp_2Fc^+/Cp_2Fc) a compound can abstract a H atom from TEMPOH, as long as the pK_a values for the reduced protonated derivatives, $[Mn^{II}(S^{Me2}N_4(tren))(ROH)]^+$ (R = H, Me, Ph, Ph^pNO_2), are greater than 18.5. The anionic thiolate of compounds **5**−**8** should increase the basicity of the coordinated oxygen in all four complexes relative to, for example, a nitrogen-ligated manganese(III) complex such as $[Mn^{III}(PY5)(OH)]^{2+}$ {**11**; PY5 = 2,6-bis[bis(2-pyridyl)methoxymethane]pyridine}.[48] Similarly, the thiolate ligand of chloroperoxidase and P450 has been shown to create a highly basic oxo that is believed to be

dx.doi.org/10.1021/ic401234t | *Inorg. Chem.* 2013, 52, 12383−12393

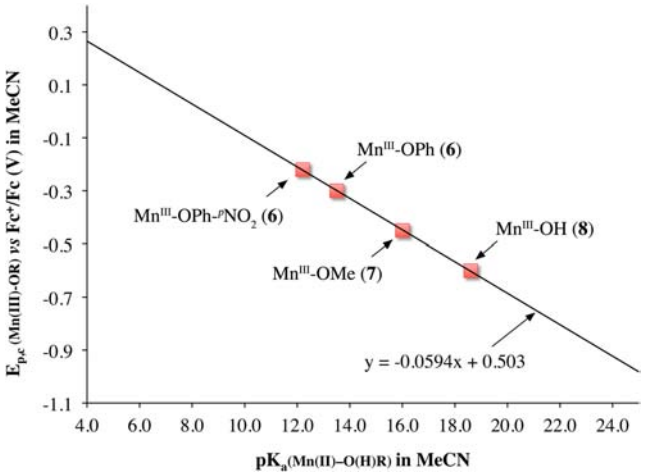

Figure 11. pK_a required to abstract a H atom from TEMPOH as a function of the redox potential in MeCN. The data points shown provide the pK_a value that would be required specifically for **5**–**8** to react with TEMPOH given their experimentally determined redox potentials.

responsible for the highly reactive nature of their mildly oxidizing active sites.[18−20] Using the estimated O−H BDFE (70.1 kcal mol^{-1}) obtained as described above for **9** in MeCN and the cathodic peak potential for **8** in MeCN (−600 mV; Table 3), we can then calculate an estimated pK_a = 21.2 for **9** using the Bordwell equation (2). This indicates that the hydroxide of thiolate-ligated **8** is approximately 8 orders of magnitude more basic than that of nitrogen-ligated **11**, the reduced protonated derivative of which has a pK_a = 13.0 ± 0.5 in the same solvent.[48] These pK_a differences, in part, reflect differences in molecular charge [1+ (**8**) vs 2+ (**11**)], as well as the electron-donating thiolate ligand present in **8** but not in **11**.[18−20] The basic hydroxy oxygen therefore allows **8**, which is nearly 1 V (780 mV) less oxidizing than **11** (+180 mV vs $Fc^{+/0}$ in MeCN), to abstract H atoms from substrates, such as TEMPOH, with weak X−H bonds. The stronger O−H bond (BDFE = 82 ± 2 kcal mol^{-1} in MeCN)[48] of the reduced protonated derivative of **11**, $[Mn^{II}(PY5)(OH_2)]^{2+}$, provides ∼12 kcal mol^{-1} more driving force relative to **8** for abstraction of the H atoms, consistent with the fact that this dicationic, N-ligated derivative abstracts H atoms from stronger X−H bonds.[48]

Although the quantitative data obtainable for **8**, because of its PCET properties in water (vide supra), are not available for methoxide-ligated **7** and phenoxide-ligated **5** and **6**, we can use the fact that the former abstract H atoms from TEMPOH, whereas the latter two do not, to place lower and upper limits on the pK_a value of the reduced protonated derivatives $Mn^{II}O(H)R$ [R = $^pNO_2Ph$, Ph, or Me (**7**)]. According to the $E_{p,c}$ versus pK_a graph of Figure 11 and the equation relating these two parameters ($E_{p,c}$= −0.0594pK_a + 0.503), we can estimate that, given their cathodic peak potentials (Table 3), the reduced protonated derivatives of phenoxide-ligated **5**, $Mn^{II}O(H)R$ (R = $^pNO_2Ph$), and **6**, $Mn^{II}O(H)R$ (R = Ph), would have to have a pK_a values of 12.2 and 13.5, respectively, in order to abstract H atoms from TEMPOH. The fact that they do not react implies that their pK_a values are less than these values (Table 3). These estimated upper limits to these pK_a values make sense given that coordination to a Mn^{3+} ion would be expected to substantially drop the pK_a of $^pNO_2PhOH$ and PhOH relative to that of the free phenols [pK_a(PhOH) = 27.2; $pK_a(^pNO_2PhOH)$ = 22][42,43] in MeCN. On the basis of its cathodic peak potential (Table 3), methoxide-ligated **7** would have to have a pK_a value of 16.2 in order to abstract H atoms from TEMPOH. The fact that **7** does, in fact, react implies that its pK_a value is greater than this.

CONCLUSIONS

In summary, we have described the synthesis, structural characterization, and electrochemical and reactivity properties of a series of thiolate-ligated $[Mn^{III}(S^{Me2}N_4(tren))(OR)]^+$ complexes [R = $^pNO_2Ph$ (**5**), Ph (**6**), Me (**7**), and H (**8**)]. Each of these complexes was synthesized via the proton-induced cleavage of a structurally characterized oxo-bridged dimer containing an unusually bent bridging Mn−O−Mn angle (158.75°) with a fairly basic oxo. An alternative route to hydroxo-bound **8** involved the aerobic oxidation of the five-coordinate manganese(II) precursor in aqueous solution. In H_2O, **8** was shown to display a pH-dependent redox potential with a Pourbaix diagram slope (52 mV pH^{-1}) that is indicative of the transfer of a single proton with each electron. The least stable, and least oxidizing members of this series, **7** and **8**, were shown to abstract H atoms from TEMPOH, whereas the more oxidizing members (based on the redox potential), **5** and **6**, were found to be unreactive. Kinetic parameters for $Mn^{III}OR$ [R = Me (**7**), H (**8**)]-promoted TEMPOH oxidation [k_H/k_D= 3.1 (**8**); k_H/k_D= 2.1 (**7**)] were shown to be consistent with concerted H-atom abstraction, and **8** was shown to react 1 order of magnitude faster than **7**. The aqueous O−H BDFE for water-bound $Mn^{II}OH_2$ (74.0 ± 0.5 kcal mol^{-1}; Table 3) was directly calculated using the best-fit line to the Pourbaix diagram in conjunction with the Bordwell equation and converted to an estimated O−H BDFE in MeCN (70.1 kcal mol^{-1}; Table 3), so that comparisons could be made with other systems. Hydroxo-bound **8** is the only water-soluble $Mn^{III}OH$ compound shown to promote HAT. It was determined that the trend in pK_a values opposes that of $E_{p,c}$ for the compounds reported herein. A pK_a value of 21.2 for the reduced protonated derivatives of **8** and **9** was calculated using the Bordwell equation and an O−H BDFE in MeCN was estimated based on its experimental value in H_2O. It was suggested that an increased oxygen basicity due to the thiolate sulfur, which offsets its low cathodic peak potential (−300 mV vs Fc^+/Fc^0), is responsible for the observed HAT reactivity of **8**. The reactivity or lack of reactivity with TEMPOH was used to place either upper or lower limits on the pK_a (Table 3) of the reduced protonated derivatives of methoxide-ligated **7** and phenoxide-ligated **5** and **6**.

ASSOCIATED CONTENT

Supporting Information

X-ray crystallographic data in CIF format for **2** and **5**–**8**, experimental details regarding the synthesis and spectroscopic characterization of **2** and **5**–**8**, reactions with TEMPOH and pK_a measurements, cyclic voltammograms of **8** in H_2O and **5**–**8** in MeCN, and kinetic plots (k_{obs} vs [TEMPOH], k_H/k_D, and Eyring plots) for the reaction between **7** and **8** and TEMPOH(D). This material is available free of charge via the Internet at http://pubs.acs.org.

AUTHOR INFORMATION

Corresponding Author

*E-mail: kovacs@chem.washington.edu. Tel.: (206)543-0713. Fax: (206)685-8665.

Notes

The authors declare no competing financial interest.

ACKNOWLEDGMENTS

NIH funding (Grant RO1GM45881-20) is gratefully acknowledged. We also thank Jeff Warren and Jim Mayer for helpful discussion.

REFERENCES

(1) Warren, J. J.; Tronic, T. A.; Mayer, J. M. *Chem. Rev.* **2010**, *110*, 6961−7001.
(2) Huynh, M. H. V.; Meyer, T. J. *Chem. Rev.* **2007**, *107*, 5004−5064.
(3) Krebs, C.; Fujimori, D. G.; Walsh, C. T.; Bollinger, J. M., Jr. *Acc. Chem. Res.* **2007**, *40*, 484−492.
(4) Arunkumar, C.; Lee, Y.-M. M.; Lee, J. Y.; Fukuzumi, S.; Nam, W. *Chem.—Eur. J.* **2009**, *15*, 11482−11489.
(5) Wang, D.; Zhang, M.; Buhlmann, P.; Que, L., Jr. *J. Am. Chem. Soc.* **2010**, *132*, 7638−7644.
(6) Lansky, D. E.; Goldberg, D. P. *Inorg. Chem.* **2006**, *45*, 5119−5125.
(7) Clark, K. B.; Culshaw, P. N.; Griller, D.; Lossing, F. P.; Simões, J. A. M.; Walton, J. C. *J. Org. Chem.* **1991**, *56*, 5535.
(8) Bordwell, F. G.; Cheng, J.-P.; Harrelson, J. A., Jr. *J. Am. Chem. Soc.* **1988**, *110*, 1229−1231.
(9) Bordwell, F. G.; Cheng, J.-P.; Ji, G. Z.; Zhang, R. *J. Am. Chem. Soc.* **1991**, *113*, 9790−9794.
(10) Mayer, J. M. *Acc. Chem. Res.* **2011**, *44*, 36−46.
(11) Wayner, D. M.; Parker, V. D. *Acc. Chem. Res.* **1993**, *26*, 287−294.
(12) Tilset, M. In *Electron Transfer in Chemistry*; Balzani, V., Ed.; Wiley-VCH: Weinheim, Germany, 2001; pp 677−713.
(13) Yin, G. *Acc. Chem. Res.* **2013**, *46*, 483−492.
(14) Wang, Y.; Sheng, J.; Shi, S.; Zhu, D.; Yin, G. *J. Phys. Chem. C* **2012**, *116*, 13231−13239.
(15) Yin, G.; Danby, A. M.; Kitko, D.; Carter, J. D.; Scheper, W. M.; Busch, D. H. *J. Am. Chem. Soc.* **2008**, *130*, 16245−16253.
(16) Yin, G.; Danby, A. M.; Kitko, D.; Carter, J. D.; Scheper, W. M.; Busch, D. H. *J. Am. Chem. Soc.* **2007**, *129*, 1512−1513.
(17) Stone, K. L.; Behan, R. K.; Green, M. T. *Proc. Natl. Acad. Sci. U.S.A.* **2006**, *103*, 12307−12310.
(18) Rittle, J.; Green, M. T. *Science* **2010**, *330*, 933−937.
(19) Green, M. T.; Dawson, J. H.; Gray, H. B. *Science* **2004**, *304*, 1653−1656.
(20) Green, M. T. *Curr. Opin. Chem. Biol.* **2009**, *13*, 84−88.
(21) Evans, D. A. *J. Chem. Soc.* **1959**, 2005.
(22) Van Geet, A. L. *Anal. Chem.* **1968**, *40*, 2227−2229.
(23) Mader, E. A.; Davidson, E. R.; Mayer, J. M. *J. Am. Chem. Soc.* **2007**, *129*, 5153−5166.
(24) Brines, L. M.; Shearer, J.; Fender, J. K.; Schweitzer, D.; Shoner, S. C.; Barnhart, D.; Kaminsky, W.; Lovell, S.; Kovacs, J. A. *Inorg. Chem.* **2007**, *46*, 9267−9277.
(25) Altomare, A.; Burla, C.; Camalli, M.; Cascarano, L.; Giacovazzo, C.; Guagliardi, A.; Moliterni, A. G. G.; Polidori, G.; Spagna, R. *J. Appl. Crystallogr.* **1999**, *32*, 115−119.
(26) Sheldrick, G. M. *SHELXL-97: Program for the Refinement of Crystal Structures*; University of Gottingen: Gottingen, Germany, 1997.
(27) Mackay, S.; Edwards, C.; Henderson, A.; Gilmore, C.; Stewart, N.; Shankland, K.; Donald, A. *MaXus: a computer program for the solution and refinement of crystal structures from diffraction data*; University of Glasgow: Glasgow, Scotland, 1997.
(28) Waasmaier, D.; Kirfel, A. *Acta Crystallogr., Sect. A* **1995**, *51*, 416.
(29) Pecoraro, V. L.; Baldwin, M. J.; Gelasco, A. *Chem. Rev.* **1994**, *94*, 807−826.
(30) Mullins, C. S.; Pecoraro, V. L. *Coord. Chem. Rev.* **2008**, *252*, 416−443.
(31) Wu, A. J.; Penner-Hahn, J. E.; Pecoraro, V. L. *Chem. Rev.* **2004**, *104*, 903−938.
(32) Baffert, C.; Collomb, M.-N.; Deronzier, A.; Pécaut, J.; Limburg, J.; Crabtree, R. H.; Brudvig, G. W. *Inorg. Chem.* **2002**, *41*, 1404−1411.
(33) Kipke, C. A.; Scott, M. J.; Gohdes, J. W.; Armstrong, W. H. *Inorg. Chem.* **1990**, *29*, 2193−2194.
(34) Horner, O.; Anxolabéhère-Mallart, E.; Charlot, M.-F.; Tchertanov, L.; Guilhem, J.; Mattioli, T. A.; Boussac, A.; Girerd, J.-J. *Inorg. Chem.* **1999**, *38*, 1222−1232.
(35) Coggins, M. K.; Toledo, S.; Shaffer, E.; Kaminsky, W.; Shearer, J.; Kovacs, J. A. *Inorg. Chem.* **2012**, *51*, 6633−6644.
(36) Mukhopadhyay, S.; Mandal, S. K.; Bhaduri, S.; Armstrong, W. H. *Chem. Rev.* **2004**, *104*, 3981−4026.
(37) Badiei, Y. M.; Siegler, M. A.; Goldberg, D. P. *J. Am. Chem. Soc.* **2011**, *133*, 1274−1277.
(38) Coggins, M. K.; Sun, X.; Kwak, Y.; Solomon, E. I.; Rybak-Akimova, E. V.; Kovacs, J. A. *J. Am. Chem. Soc.* **2013**, *135*, 5631−5640.
(39) Theisen, R. M.; Shearer, J.; Kaminsky, W.; Kovacs, J. A. *Inorg. Chem.* **2004**, *43*, 7682−7690.
(40) Gupta, R.; Borovik, A. S. *J. Am. Chem. Soc.* **2003**, *125*, 13234−13242.
(41) Yin, G.; McCormick, J. M.; Buchalova, M.; Danby, A. M.; Rogers, K.; Day, V. W.; Smith, K.; Perkins, C. M.; Kitko, D.; Carter, J. D.; Scheper, W. M.; Busch, D. H. *Inorg. Chem.* **2006**, *45*, 8052−8061.
(42) Izutsu, K. *Acid−Base Dissociation Constants in Dipolar Aprotic Solvents*; Blackwell Scientific: Oxford, England, 1990; Vol. 35.
(43) Kolthoff, I. M.; Chantooni, M. K.; Bhowmik, S. *J. Am. Chem. Soc.* **1968**, *90*, 23−28.
(44) Armstrong, W. H.; Lippard, S. J. *J. Am. Chem. Soc.* **1984**, *106*, 4632−4633.
(45) Carroll, M. M.; Norton, J. R. *J. Am. Chem. Soc.* **1992**, *114*, 8744−8745.
(46) Ghosh, K.; Eroy-Reveles, A. A.; Olmstead, M. M.; Mascharak, P. K. *Inorg. Chem.* **2005**, *44*, 8469−8475.
(47) Shirin, Z.; Young, V. G., Jr.; Borovik, A. S. *Chem. Commun.* **1997**, 1967−1968.
(48) Goldsmith, C. R.; Cole, A. P.; Stack, T. D. P. *J. Am. Chem. Soc.* **2005**, *127*, 9904−9912.
(49) Hubin, T. J.; McCormick, J. M.; Collinson, S. R.; Buchalova, M.; Perkins, C. M.; Alcock, N. W.; Kahol, P. K.; Raghunathan, A.; Busch, D. H. *J. Am. Chem. Soc.* **2000**, *122*, 2512−2522.
(50) Shirin, Z.; Hammes, B. S.; Young, V. G.; Borovik, A. S. *J. Am. Chem. Soc.* **2000**, *122*, 1836−1837.
(51) Lugo-Mas, P.; Dey, A.; Xu, L.; Davin, S. D.; Benedict, J.; Kaminsky, W.; Hodgson, K. O.; Hedman, B.; Solomon, E. I.; Kovacs, J. A. *J. Am. Chem. Soc.* **2006**, *128*, 11211−11221.
(52) Swartz, R. D.; Coggins, M. K.; Kaminsky, W.; Kovacs, J. A. *J. Am. Chem. Soc.* **2011**, *133*, 3954−3963.
(53) Brines, L. M.; Villar-Acevedo, G.; Kitagawa, T.; Swartz, R. D.; Lugo-Mas, P.; Kaminsky, W.; Benedict, J. B.; Kovacs, J. A. *Inorg. Chim. Acta* **2008**, *361*, 1070−1078.
(54) Yano, J.; Kern, J.; Sauer, K.; Latimer, M.; Pushkar, Y.; Biesiadka, J.; Loll, B.; Saenger, W.; Messigner, J.; Zouni, A.; Yachandra, V. K. *Science* **2006**, *314*, 821−825.
(55) Dismukes, G. C.; Brimblecombe, R.; Felton, G. A. N.; Pryadun, R. S.; Sheats, J. E.; Spiccia, L.; Swiegers, G. F. *Acc. Chem. Res.* **2009**, *42*, 1935−1943.
(56) Yachandra, V. K.; Sauer, K.; Klein, M. P. *Chem. Rev.* **1996**, *96*, 2927−2950.
(57) Brines, L. M.; Villar-Acevedo, G.; Kitagawa, T.; Swartz, R. D.; Lugo-Mas, P.; Kaminsky, W.; Benedict, J. B.; Kovacs, J. A. *Inorg. Chim. Acta* **2008**, *361*, 1070−1078.